Bulletin of Electrical Engineering and Informatics
Vol. 15, No. 1, February 2026, pp. 327~337
ISSN: 2302-9285, DOI: 10.11591/eei.v15i1.10447

Improved feature-based hybrid deep learning for multiclassification of ultrasound thyroid nodules

Mayuresh Gulame[1], Deepthi D. Kulkarni[2], Priya Khune[1], Nilesh N. Thorat[1], Ashwini G. Shahapurkar[1], Vijaya S. Patil[1], Sumit Arun Hirve[1], Aarti Pimpalkar[1]
[1]Department of Computer Engineering, School of Computing, MIT Art, Design and Technology University, Pune, India
[2]Department of Electronics and Telecommunication Engineering, KJEI's Trinity Academy of Engineering, Pune, India

Article Info

Article history:

Received Apr 10, 2025
Revised Oct 3, 2025
Accepted Dec 6, 2025

Keywords:

Deep learning
Local ternary patterns and multitexton features
Thyroid imaging reporting and data system score
Thyroid nodules
U-Net segmentation

ABSTRACT

Ultrasonography is frequently used to identify thyroid nodules. Because of their internal features, variable appearances, and ill-defined borders, it might be difficult for a hospitalist to distinguish amongst benign and malignant forms of the nodule based solely on visual inspection. Although deep learning (DL), a subset of artificial intelligence, has significantly advanced medical image recognition, challenges remain in achieving accurate and efficient diagnosis of thyroid nodules. To identify and classify thyroid nodules, this study uses an innovative hybrid DL-assisted multi-classification technique. A median blur eliminates salt-and-pepper noise, and this is followed by segmentation using a method based on enhanced pooling integrated U-Net (EPIU-Net). To produce a single histogram series, features are recovered from the segmented image, including multi-texton, and local ternary pattern (LTP) based patterns. Following feature extraction, the data is expanded and input into a fusion classification model utilizing Deep Maxout and convolutional neural network (CNN) to categorize nodules. This work uses 2 types of datasets and for both datasets, we achieved great results with our hybrid technique across all performance criteria. 0.976, 0.008, 0.992, and 0.017 are the corresponding values for accuracy, false discovery rate (FDR), sensitivity, and false negative rate (FNR). Moreover proposed work is verified by k-fold method.

Corresponding Author:

Mayuresh Gulame
Department of Computer Engineering, School of Computing
MIT Art, Design and Technology University
MIT ADT Campus, Loni Kalbhor, Pune–Solapur Highway, Pune 412201, Maharashtra, India
Email: mayuresh2103@gmail.com

1. INTRODUCTION

One's health may be jeopardized by thyroid nodules, which can develop into among the most prevalent and deadly kinds of cancer. One since the precise cause of thyroid nodules has not been established, early detection and therapy alone may increase the chances of successfully treating thyroid cancer. Clinical evaluation of thyroid lumps is challenging. Their prevalence rises with age, with 42–76% of people potentially having them [1]. Depending on the histological subtype, patient preferences, and comorbidities, treatment options for thyroid tumor may include thyroidectomy, immunotherapy, radioactive iodine therapy, or chemoradiotherapy to prevent mortality and recurrence. The overwhelming majority of thyroid nodules are non-malignant, but 10% have the potential to be malignant. A uniform grading system predicated on the features of nodule ultrasound such size, borders, calcification, internal composition, and echogenicity allows radiologists to report on the probability that thyroid nodules are cancerous [2].

Clinical diagnosis of thyroid nodules, ultrasonography continues to be the most widely used and advised screening method. Ultrasonography is a non-invasive, low-cost method of imaging the thyroid gland, and surrounding tissue. Furthermore, although still quite subjective and substantially dependent on radiologists' clinical expertise, the sonographic diagnosis of thyroid knot has typically been based on evidence-based imaging results. The diagnosis is made with fine-needle aspiration biopsy (FNAB) in conjunction with follow-up therapy [3]. Physicians frequently use their personal knowledge to make clinical diagnoses of thyroid nodules. But using this method might lead to an inaccurate identification, which would then necessitate needless procedures such a biopsy and surgery. There is a need for systems that can accurately distinguish between individuals with thyroid nodules that are benign or cancerous. Artificial intelligence (AI) methodology are crucial in the diagnosis of diseases in biomedical images, and computer-aided diagnosis (CAD) systems are the preferred solution for addressing this issue. Computer systems that can help with thyroid nodule radiological classification can incorporate described thyroid imaging reporting and data systems (TI-RADS) properties [4].

In various illness diagnosis models, deep learning (DL) is one of them that has advanced rapidly over the past few decades. Also developed and producing good results is a unique cascaded convolutional neural network (CNN) that makes thyroid nodule identification possible. To handle the diagnosis model more effectively and accurately, this work is to introduce the deep hybrid technique for precise thyroid nodule diagnosis along with proposed segmentation and feature extraction. The paper's contribution and structure are as follows:

a. Aiming to segment the image, the enhanced pooling integrated U-Net (EPIU-Net)-based segmentation model ensures the high dice coefficient and intersection over union (IoU) of the segmented image and which will be useful for further processing.
b. Putting forth the idea of using local ternary pattern (LTP)-and improved multi-texton-based features that were taken from the segmented image. These extracted features will be used for classification.
c. Using Deep Maxout+CNN to classify the type of malignant thyroid in the multiclass classification.
d. The classification performance is evaluated by K-fold method.

2. LITERATURE SURVEY

Using the applied network hyperparameters and loss function regularization, Cho *et al*. [5] created a novel deep neural network (DNN) framework to carry out nodule identification. This approach was executed without considering intricate post-processing enhancement stages. Moreover, the outlined model identified the various types of thyroid nodules and enhanced the segmentation technique's prediction precision.

Park *et al*. [6] verified that radiography and CAD were typically equivalent; it is possible for CAD to help physicians diagnose patients. Pimpalka and Jagtap [7] selected six features, computed the F-score of these feature sets, and used support vector machines (SVMs) to filter out the key texture characteristics in preparation for further. Gray-level co-occurrence matrix (GLCM) was used by Lyra *et al*. [8] to describe the textural properties of thyroid nodules. Another attempt to categorize thyroid nodules, Keramidas *et al*. [9] employed by local binary patterns (LBPs) for extraction of features of nodules.

A DL framework for feature extraction from sonography pictures was outlined by Chi *et al*. [10] through testing on their own database, the suggested model demonstrated 96.34% accuracy, 86% sensitivity, and 99% specificity. Peng *et al*. [11] created a ThyNet model to categorize thyroid lumps from various medical facilities; the model's area under the receiver operating characteristic curve (AUROC) was 0.922. In the hypothetical scenario, the frequency of fine-needle aspiration (FNA) decreases and the percentage of malignant tumors ignored for diagnosis drops from 18.9% to 17% [11].

Ma *et al*. [12] employed two pretrained CNNs to label thyroid lumps; the CNNs' feature maps were then concatenated. With the CNN model they had learned from ImageNet, Liu *et al*. [13] pretrainedly extracted features utilizing a fresh dataset of sonography images. The suggested technique created a hybrid feature space by combining high-level deep features from CNN models with conventional low-level features taken from the histogram of oriented gradient (HOG) and LBP, 93.10% [13] was the accuracy of the experiment.

Moreover, Chen *et al*. [14] employed a DL ultrasound text classifier to forecast thyroid lesions. On standard datasets and genuine medical datasets, the method's accuracy was 95% and 93%. The literature review highlights the need for more sophisticated, data-driven methods for classifying thyroid nodules. This research will concentrate on creating a novel classification model that overcomes existing constraints and improves diagnostic accuracy.

3. PROPOSED METHOD

Thyroid nodules must be identified and evaluated as soon as possible. Human inspection has been the primary method of identifying thyroid nodules. But using this method makes it challenging to recognize thyroid nodules in ultrasound images. A foremost drawback of the handmade features scheme is that it is not universally applicable due to its high complexity. Figure 1 illustrates the proposed thyroid nodule detection model's configuration which will give tremendous classification of thyroid lumps.

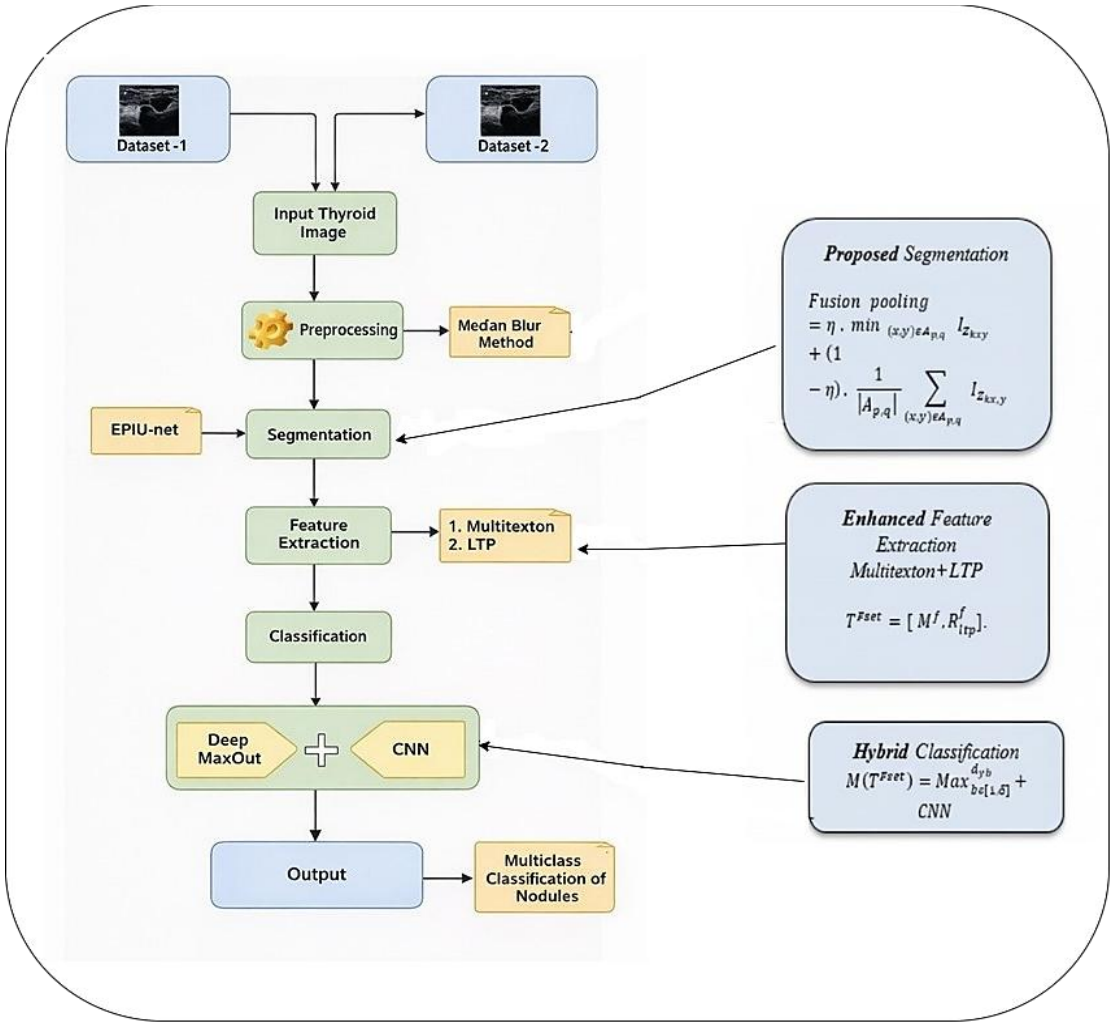

Figure 1. Proposed thyroid nodule detection model's configuration

In order to extract multi-texton features, and LTP-based features, the input picture must first be preprocessed using the median blur technique before being sent into the EPIU-Net model for image segmentation. Additionally, digital database of thyroid ultrasound images (DDTI) data was augmented and then fed into a nodule classification model. CNN and the hybrid classifier Deep Maxout train the features and forecast the output that is observed.

3.1. Pre-processing

Considering the pair of datasets, DDTI and Dataset 2, where *I* is the representation of the first image. To obtain the proper denoised image for additional processing, the image is first preprocessed. There may be some noise in US picture *I* during the capture and transfer process. This noise causes random dark or bright noise pixels to appear on image *I*, which modifies the visual effects of the image. This effort utilizes the median blur method [15] to remove the undesired noise from image *I*. Later on, these pixels are substituted as the median; in contrast, the center value is regarded as the median, rejecting the window's noisy pixels. The preprocessed picture is thus formed with a dimension of 256*256 and can be denoted as I_{Pre} when the image size decreases.

3.2. Enhanced pooling integrated U-Net segmentation

First, salt and pepper noise are removed from the ultrasonic image by using a median filter. We feed our segmentation block with this previously processed image. An improved U-net segmentation procedure is applied to this image [16]. The accompanying Figure 2 illustrates the flow of our EPIU-Net technique where we have used mixed pooling to heighten segmentation of thyroid tumors.

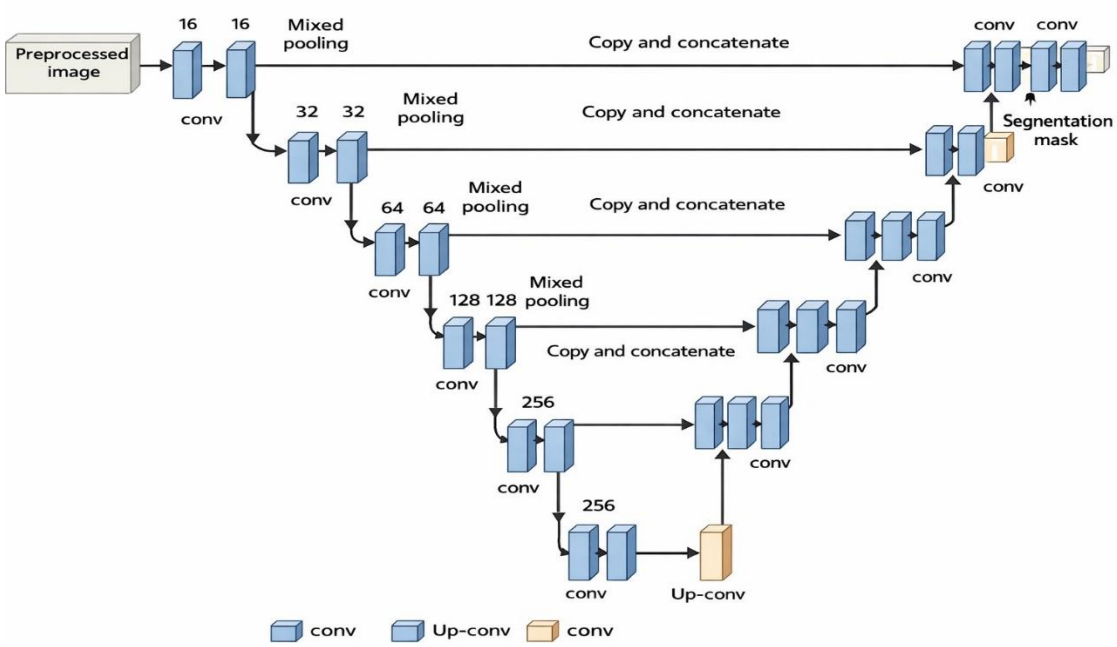

Figure 2. Suggested technique for segmenting thyroid lumps

The approach makes use of a network of encoders. Four encoder blocks make up this encoder network. A Leaky rectified linear unit (ReLU) activation function is followed by two convolutional layers, all with a 3*3 kernel dimension and the proper padding. A 2*2 kernel dimension is used to feed this into a mixed pooling layer. By reducing the model training's computational cost is cut in half, the mixed pooling layer lowers the learned spatial dimensions. The EPIU-Net states as (1):

$$Fusion\ pooling = \eta\ .\ min\ _{(x,y)\epsilon A_{p,q}} I_{Z_{kxy}} + (1-\eta).\frac{1}{|A_{p,q}|}\sum_{(x,y)\epsilon A_{p,q}} I_{Z_{kx,y}} \quad (1)$$

Where, $I_{Z_{(p,q)}}$ is the pixel significance of x-th row and y-th column of image I_z, η signifies arbitrary value in the interval [0, 1], $|A_{p,q}|$ is the pooling area dimension, and m and n are the width and height of the image I_z, correspondingly [17].

3.3. Feature extraction: multi-texton and local ternary pattern

3.3.1. Multitexton features

With the usage of multi-texton based features, this learning extracts the texton image from the segmented image I_{seg} that has the texture orientation and vertical color correlation. Color histograms and co-occurrence matrices are provided by the multi-texton features that identify diverse images. A range of textons are accepted plus joined with the produced maps on the segmented image I_{seg}. Furthermore, due of the texture orientation, the texton image has a semantic description. In this case, ω represents the texture orientation, and f_h and f_v are the maps made in the horizontal and vertical directions, respectively [17]. Using multi-texton based features, this learning extracts the texton image from the segmented image I_{seg} with the texture orientation and the spatial correlation of colors. Multi-texton features offer co-occurrence matrix and color histogram functionality in addition to being used to identify heterogeneous images. It is allowed to mix the range of textons on the segmented picture I_{seg} with the created maps. Because of the texture orientation, the texton picture also has a semantic definition. Furthermore, for the gray-level image delivered by (2), a

texture orientation $_{\omega}$ map is ready. In this instance, the texture orientation is shown, and the maps were made in both horizontal f_h and f_v vertical directions.

$$\omega = arctan\frac{f_v}{f_h} \quad (2)$$

Once more, because it is unproductive and drops added information, the texture orientation map directed above is substituted. The improved process is then provided in (3) to extract the texture orientation from the color image. The gradient maps shown here are for the horizontal and vertical directions, respectively.

$$\omega = arccos\frac{x.y}{|x|.|y|} \quad (3)$$

In the RGB color system, the gradient map is created for the red channel and the values of $|x|.|y|$ and $x.y$ are as in (4):

$$|x| = \sqrt{{R_h}^2 + {G_h}^2 + {B_h}^2}$$

$$|y| = \sqrt{{R_v}^2 + {G_v}^2 + {B_v}^2}$$

$$x.y = R_h.R_v + G_h.G_v + B_h.B_v \quad (4)$$

Then the multi-texton based features can be signified as M^f.

3.3.2. Local ternary pattern features

Based on LTP, this learning extracts characteristics from a segmented picture I_{seg}. The values 0 and 1 are utilized in the LTP, an expanded version of LBP. When the threshold T_h is set to the ternary code, it can have one of three values (-1, 0, 1). The threshold T_h is taken into attention and the gray values of the pixels in the region are accustomed within the range of (-1, 0, 1) based on the value of the essential pixel [18].

Gray levels $G_c - T_h$ below the threshold are counted as -1, those above the threshold $G_c - T_h$ as +1, and those below the threshold G_c as 0 are counted as 0. In that case, the LTP code formulation can be described as in (5). The core pixel G_c, the threshold T_h, and G_c the neighboring gray level of the pixel are shown here.

$$G(G_p, G_c, T_h) = \begin{cases} +1, G_p \geq G_c + T_h \\ 0, |G_p - G_c| < T_h \\ -1, G_p \leq G_c - T_h \end{cases} \quad (5)$$

As a result, the codes for the lower and upper LTPs can be found in (6). These are the upper LTP is Up_{ltp} and the lower LTP is Lo_{ltp}, respectively.

$$Lo_{ltp} = \sum_{p=0}^{7} 2p\varphi(G_p - G_c - T_h)$$

$$Up_{ltp} = \sum_{p=0}^{7} 2p\varphi(G_p - G_c - T_h) \quad (6)$$

Lastly, the Up_{ltp} and Lo_{ltp} are coupled together to get the resulting future vector as R_{ltp}^f. Thus, the whole features extracted from the segmented image can be symbolized as:

$$T^{Fset} = [M^f, R_{ltp}^f].$$

3.4. Proposed hybrid classification and thyroid imaging reporting and data system score classification

The hybrid classifier, which combines CNN and Deep Maxout, uses the feature set T^{Fset} that was extracted from the image I_{seg} to expedite the nodule classification process. After training the extracted feature set, the classifiers Deep Maxout and CNN produce the scores (intermediate result). Then, based on these hybrid classifier results, a binary prediction of 0 or 1 indicates whether the provided image is benign or

cancerious. The subsequent procedure examines the thyroid imaging reporting and data system (TIRADS) score [19] classification type after the cancerous thyroid has been discovered.

3.4.1. Deep Maxout

In order to determine if a thyroid is benign or cancerous, the Deep Maxout model trains the feature set T^{Fset}. Seven layers make up the Deep Maxout structure as well: input, embedding, max pooling, dropout, and output layers with activation and maxout functions. First and foremost, the Maxout and Dropout layers advance the categorization process's usefulness [20], [21]. Likewise, the activation function's deployment strengthens the recommended thyroid lump classification. In (7) can be used to indicate the Maxout unit. Here, $d_{yb} = T^{Fset}.\psi_{yb} + \chi_{yb}$, ψ denotes weight, χ denotes bias term and δ denotes features map:

$$M(T^{Fset}) = Max_{b\epsilon[1,\delta]}^{d_{yb}} \tag{7}$$

Consequently, the Deep Maxout classifier's intermediate findings can be expressed as Max^{Out}.

3.4.2. Convolutional neural network

CNNs are outstanding at differentiating between benign and malignant nodules by training on extensive datasets, thereby minimizing the necessity for invasive procedures and improving diagnostic accuracy. The CNN design is made up of an output layer, one or more fully linked layers, and diverse or unique sub-sampling and convolution layers. This classifier is utilized to train the extracted feature set in order to conclude the presence or absence of a thyroid lump malignancy [22], [23].

4. RESULT AND DISCUSSION

4.1. Dataset used

For the scientific community, the DDTI database is an open access resource. Enhancing the development of algorithms which is used in CAD systems for thyroid nodule analysis many researchers using this dataset [24]. DDTI dataset consist of 134 images with TIRADS score labelling. Generative adversarial network (GAN)-based synthesis, diffusion models is used to generate realistic ultrasound variations up to 1340 images. Algerian Ultrasound Images Thyroid Dataset (AUITD) is the name of Dataset 2. Where the information was gathered from hospitals in Setif, Algeria, and labelled by medical professionals who volunteered their services. Additionally, it is divided into three classes: benign thyroid (171 photos), malignant thyroid (1,895 images), and normal thyroid (1,895 images) [25].

4.2. Improved segmentation (enhanced pooling integrated U-Net) results

Figure 3 shows comparison of EPIU method with existing segmentation technologies. This figure relates segmentation outcomes on medicinal images utilizing diverse practices. It illustrates how Figure 3(a) original US image, Figure 3(b) U-NET, Figure 3(c) FCM, Figure 3(d) K-means, and Figure 3(e) EPIU-Net ways vary in identifying regions of interest related to the original sample images.

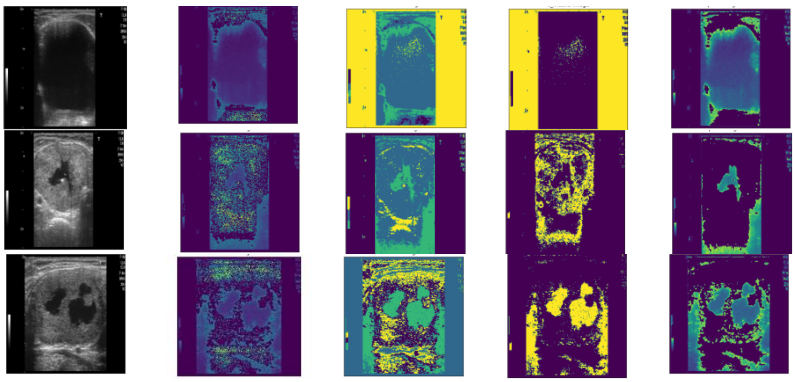

Figure 3. Assessment of segmentation strategy; (a) sample image, (b) U-NET, (c) FCM, (d) K-means, and (e) EPIU-Net

4.3. Impact on hybrid model utilizing the database of thyroid ultrasound images dataset and Dataset 2

Here, we have used two distinct datasets to examine the effects on the hybrid model, which is presented in Table 1. Following tables compares, the model with conventional segmentation, model with conventional features, and model without feature extraction and model with our hybrid techniques. Eventually our model acquired owing outcome for diverse measures. Figure 4 illustrate graphical representation of performance measures shows how our proposed work will get good result for both datasets.

Table 1. Impact on hybrid model using DDTI dataset

Methods	Hybrid model	Model employing traditional segmentation	Model with traditional features	Model without feature extraction
Accuracy	0.971	0.858	0.915	0.892
False discovery rate (FDR)	0.017	0.131	0.105	0.128
Sensitivity	0.993	0.890	0.932	0.903
Matthews correlation coefficient (MCC)	0.973	0.767	0.830	0.754
Specificity	0.980	0.885	0.897	0.909
Precision	0.973	0.849	0.904	0.882
False positive rate (FPR)	0.019	0.185	0.153	0.191
F-measure	0.973	0.884	0.928	0.907
False negative rate (FNR)	0.017	0.141	0.088	0.097

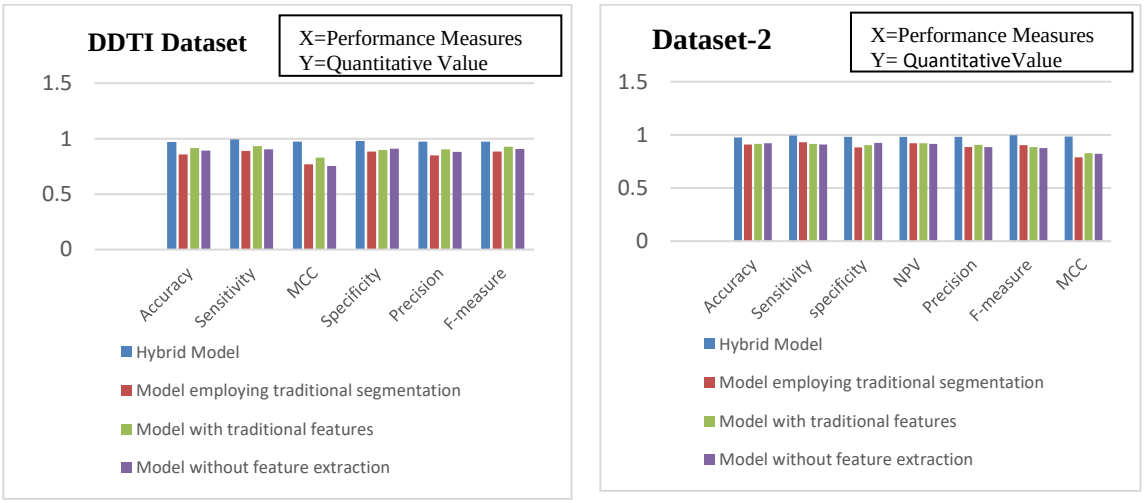

Figure 4. Comparison of hybrid method with SOA methods

4.4. Analysis by K-fold strategy

The K-fold exploration shown in Table 2. In comparison with existing approaches such as deep convolutional neural network (DCNN), you only look once version 3 (YOLOV3), CNN, deep belief network (DBN), bidirectional gated recurrent unit (Bi-GRU), Deep Maxout, and recurrent neural network (RNN), the suggested model has a high accuracy (0.989). The results demonstrate that the TIRADS score is successfully classified using the proposed methodology which greatly outperformed the previous approaches for diagnosing thyroid nodules using hybrid classifiers like Deep Maxout and CNN. Table 2 shows our proposed system is excellent over SAO method on every performance measures. Figure 5 demonstrate the comparison of our suggested system with SOA method which has got exceptional performance.

Table 2. K-fold analysis of proposed method with SOA method

Methods	YOLOV3	CNN	DBN	BI_GRU	Deep-Maxout	RNN	Proposed hybrid model
NPV	0.856	0.847	0.856	0.872	0.813	0.865	0.976
FNR	0.130	0.128	0.112	0.119	0.108	0.119	0.023
Specificity	0.876	0.871	0.894	0.886	0.836	0.895	0.987
NPV	0.102	0.101	0.105	0.127	0.113	0.158	0.011
Precision	0.876	0.889	0.855	0.832	0.865	0.909	0.983
Accuracy	0.880	0.873	0.891	0.871	0.890	0.812	0.989
MCC	0.789	0.754	0.799	0.708	0.779	0.808	0.974
Sensitivity	0.888	0.840	0.872	0.892	0.865	0.865	0.983
F_measure	0.854	0.834	0.898	0.871	0.890	0.849	0.986

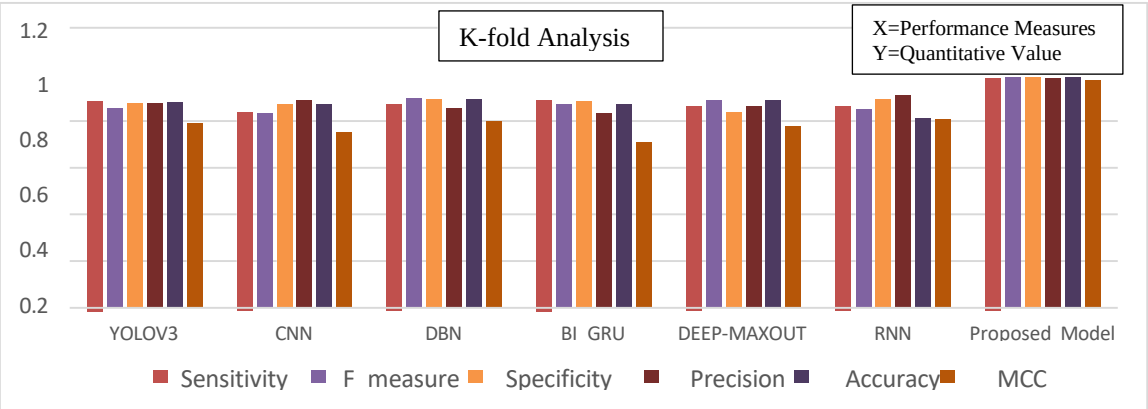

Figure 5. Comparison of proposed hybrid method with SOA methods

5. CONCLUSION

To ascertain and categorize thyroid lumps, this learning illustrate an innovative hybrid DL aided multi-classification method. The median blur method was utilized to get a crisp image by confiscating the noise from the salt and pepper. The assembly of segments was then developed utilizing segmentation built on EPIU-Net. From the segmented image, features including multitexton and LTP-based feature extraction is utilized. Following feature extraction, the DDTI dataset's data augmentation procedure was used. The features were then supplied to a hybrid classification-based lump classification model, which combines CNN and Deep Maxout. Furthermore, model trained the features and predicted the thyroid nodules. Our hybrid method got excellent result for all performance measures for both datasets. Accuracy, FDR, sensitivity, FNR, specificity, NPV, precision, F-measure, and FPR are 0.976, 0.008, 0.992, 0.017, 0.981, 0.982, 0.981, 0.997, and 0.009 respectively. This showed that the suggested scheme for classifying thyroid nodules using hybrid classifiers like CNN and Deep Maxout considerably outperformed earlier methods. Moreover the proposed method has been evaluated by K-fold method which has got accuracy is 98.9%. Upcoming studies may utilize larger multi-center datasets and transformer-driven hybrid approaches. Clinical validation in real-world settings will be crucial to confirm robustness and practical effectiveness in thyroid nodule classification.

FUNDING INFORMATION

The work in this manuscript did not receive any research funding/grant.

AUTHOR CONTRIBUTIONS STATEMENT

This journal uses the Contributor Roles Taxonomy (CRediT) to recognize individual author contributions, reduce authorship disputes, and facilitate collaboration.

Name of Author	C	M	So	Va	Fo	I	R	D	O	E	Vi	Su	P	Fu
Mayuresh Gulame	✓	✓							✓	✓				
Deepthi D. Kulkarni	✓	✓							✓	✓		✓		
Priya Khune	✓	✓	✓					✓	✓	✓				
Nilesh N. Thorat	✓	✓			✓	✓			✓	✓				
Ashwini G. Shahapurkar	✓	✓		✓					✓	✓	✓			
Vijaya S. Patil	✓	✓							✓	✓				
Sumit Arun Hirve	✓	✓	✓						✓	✓			✓	
Aarti Pimpalkar	✓	✓			✓				✓	✓		✓		

C : **C**onceptualization
M : **M**ethodology
So : **So**ftware
Va : **Va**lidation
Fo : **Fo**rmal analysis
I : **I**nvestigation
R : **R**esources
D : **D**ata Curation
O : Writing - **O**riginal Draft
E : Writing - Review & **E**diting
Vi : **Vi**sualization
Su : **Su**pervision
P : **P**roject administration
Fu : **Fu**nding acquisition

CONFLICT OF INTEREST STATEMENT

Authors state no conflict of interest.

DATA AVAILABILITY

Data availability is not applicable to this paper as no new data were created or analyzed in this study.

REFERENCES

[1] D. Fresilli *et al.*, "Thyroid Nodule Characterization: How to Assess the Malignancy Risk. Update of the Literature," *Diagnostics*, vol. 11, no. 8, p. 1374, Jul. 2021, doi: 10.3390/diagnostics11081374.

[2] M. Itani, R. Assaker, M. Moshiri, T. J. Dubinsky, and M. K. Dighe, "Inter-observer Variability in the American College of Radiology Thyroid Imaging Reporting and Data System: In-Depth Analysis and Areas for Improvement," *Ultrasound in Medicine & Biology*, vol. 45, no. 2, pp. 461–470, Feb. 2019, doi: 10.1016/j.ultrasmedbio.2018.09.026.

[3] S. De Vincentis *et al.*, "Value of repeated US-guided fine-needle aspiration (US-FNAB) in the follow-up of benign thyroid nodules: a real-life study based on the MoCyThy (Modena's Cytology of the Thyroid) DATABASE with a revision of the literature," *Endocrine*, vol. 84, no. 1, pp. 193–202, Dec. 2023, doi: 10.1007/s12020-023-03641-y.

[4] F. Bini *et al.*, "Artificial Intelligence in Thyroid Field—A Comprehensive Review," *Cancers*, vol. 13, no. 19, pp. 1-18, Sep. 2021, doi: 10.3390/cancers13194740.

[5] H. Cho, Y. Kim, E. Lee, D. Choi, Y. Lee, and W. Rhee, "Basic Enhancement Strategies When Using Bayesian Optimization for Hyperparameter Tuning of Deep Neural Networks," *IEEE Access*, vol. 8, pp. 52588–52608, 2020, doi: 10.1109/ACCESS.2020.2981072.

[6] V. Y. Park *et al.*, "Diagnosis of Thyroid Nodules: Performance of a Deep Learning Convolutional Neural Network Model vs. Radiologists," *Scientific Reports*, vol. 9, no. 1, pp.1-9, Nov. 2019, doi: 10.1038/s41598-019-54434-1.

[7] A. P. Pimpalkar and A. Jagtap, "Plant disorder recognition and classification with segmentation," in *Progressive Computational Intelligence, Information Technology and Networking*, London: CRC Press, 2025, pp. 53–58, doi: 10.1201/9781003650010-8.

[8] M. E. Lyra *et al.*, "Texture characterization in ultasonograms of the thyroid gland," in *Proceedings of the 10th IEEE International Conference on Information Technology and Applications in Biomedicine*, IEEE, Nov. 2010, pp. 1–4, doi: 10.1109/ITAB.2010.5687628.

[9] E. G. Keramidas, D. K. Iakovidis, D. Maroulis, and S. Karkanis, "Efficient and Effective Ultrasound Image Analysis Scheme for Thyroid Nodule Detection," in *Image Analysis and Recognition*, Berlin, Heidelberg: Springer Berlin Heidelberg, 2007, pp. 1052–1060, doi: 10.1007/978-3-540-74260-9_93.

[10] J. Chi, E. Walia, P. Babyn, J. Wang, G. Groot, and M. Eramian, "Thyroid Nodule Classification in Ultrasound Images by Fine-Tuning Deep Convolutional Neural Network," *Journal of Digital Imaging*, vol. 30, no. 4, pp. 477–486, Aug. 2017, doi: 10.1007/s10278-017-9997-y.

[11] S. Peng *et al.*, "Deep learning-based artificial intelligence model to assist thyroid nodule diagnosis and management: a multicentre diagnostic study," *The Lancet Digital Health*, vol. 3, no. 4, pp. e250–e259, 2021, doi: 10.1016/S2589- 7500(21)00041-8.

[12] J. Ma, F. Wu, J. Zhu, D. Xu, and D. Kong, "A pre-trained convolutional neural network based method for thyroid nodule diagnosis," *Ultrasonics*, vol. 73, pp. 221–230, Jan. 2017, doi: 10.1016/j.ultras.2016.09.011.

[13] T. Liu, S. Xie, J. Yu, L. Niu, and W. Sun, "Classification of thyroid nodules in ultrasound images using deep model based transfer learning and hybrid features," in *2017 IEEE International Conference on Acoustics, Speech and Signal Processing (ICASSP)*, IEEE, Mar. 2017, pp. 919–923, doi: 10.1109/ICASSP.2017.7952290.

[14] D. Chen, J. Niu, Q. Pan, Y. Li, and M. Wang, "A Deep-Learning Based Ultrasound Text Classifier for Predicting Benign and Malignant Thyroid Nodules," in *2017 International Conference on Green Informatics (ICGI)*, IEEE, Aug. 2017, pp. 199–204, doi: 10.1109/ICGI.2017.39.

[15] H. A. Nugroho, E. L. Frannita, A. Nugroho, Zulfanahri, I. Ardiyanto, and L. Choridah, "Classification of thyroid nodules based on analysis of margin characteristic," in *2017 International Conference on Computer, Control, Informatics and its Applications (IC3INA)*, IEEE, Oct. 2017, pp. 47–51, doi: 10.1109/IC3INA.2017.8251738.

[16] A. P. Pimpalkar and A. M. Jagtap, "Plant Disease Detection: PyramidNet-ICNN Architecture With Modified BIRCH Segmentation," *Journal of Phytopathology*, vol. 173, no. 3, May 2025, doi: 10.1111/jph.70068.

[17] Y. S. Kumari, V. V. Kumar, and C. Satyanarayana, "Texture Classification Using Complete Texton Matrix," *International Journal of Image, Graphics and Signal Processing*, vol. 9, no. 10, pp. 60–68, Oct. 2017, doi: 10.5815/ijigsp.2017.10.07.

[18] E. Akanksha and P. Rao, "A Feature Extraction Approach for Multi-Object Detection Using HoG and LTP," *International Journal of Intelligent Engineering and Systems*, vol. 14, no. 5, pp. 259–268, Oct. 2021, doi: 10.22266/ijies2021.1031.24.

[19] L. Gao *et al.*, "Comparison among TIRADS (ACR TI-RADS and KWAK- TI-RADS) and 2015 ATA Guidelines in the diagnostic efficiency of thyroid nodules," *Endocrine*, vol. 64, no. 1, pp. 90–96, Apr. 2019, doi: 10.1007/s12020-019-01843-x.

[20] Z. Zhou, Y. Wang, J. Yu, W. Guo, and Z. Li, "Super-Resolution Reconstruction of Plane-Wave Ultrasound Image Based on a Multi-Angle Parallel U-Net with Maxout Unit and Novel Loss Function," *Journal of Medical Imaging and Health Informatics*, vol. 9, no. 1, pp. 109–118, Jan. 2019, doi: 10.1166/jmihi.2019.2548.

[21] K. Balaji and K. Lavanya, "Medical Image Analysis With Deep Neural Networks," in *Deep Learning and Parallel Computing Environment for Bioengineering Systems*, 2019, pp. 75–97, doi: 10.1016/B978-0-12-816718-2.00012-9.

[22] W. Li, S. Cheng, K. Qian, K. Yue, and H. Liu, "Automatic Recognition and Classification System of Thyroid Nodules in CT Images Based on CNN," *Computational Intelligence and Neuroscience*, vol. 2021, no. 1, Jan. 2021, doi: 10.1155/2021/5540186.

[23] L. Wang *et al.*, "A Multi-Scale Densely Connected Convolutional Neural Network for Automated Thyroid Nodule Classification," *Frontiers in Neuroscience*, vol. 16, May 2022, doi: 10.3389/fnins.2022.878718.

[24] L. Pedraza, C. Vargas, F. Narváez, O. Durán, E. Muñoz, and E. Romero, "An open access thyroid ultrasound image database," in *10th International Symposium on Medical Information Processing and Analysis*, Jan. 2015, p. 92870W, doi: 10.1117/12.2073532.

[25] J. Kumar, S. N. Panda, and D. Dayal, "Utilizing Deep Learning Models for the Classification of Thyroid Nodules in Ultrasound Image," *The International Journal of Engineering and Science (IJES)*, vol. 12, no. 11, pp. 18–31, 2023, doi: 10.9790/1813-12111831.

BIOGRAPHIES OF AUTHORS

Dr. Mayuresh Gulame awarded Ph.D. in image Processing in 2025 from SPPU Pune also M.E. degree from SPPU in 2013 in signal processing. He is working as Assistant Professor in MIT Art, Design and Technology University, Pune, Maharashtra, India. He has having 13 yrs of teaching experience. His research areas include biomedical image processing, signal processing, machine learning, and deep learning. He can be contacted at email: mayuresh2103@gmail.com.

Deepthi D. Kulkarni (Ph.D. in Electronics and Telecommunication, SPPU University) is an Associate Professor in the Department of Electronics and Telecommunication Engineering at Trinity Academy of Engineering, Pune. With over 18 years of teaching and industry experience, she has contributed extensively to research in bio-medical, artificial intelligence, and machine learning. She can be contacted at email: deepthi.me2009@gmail.com.

Priya Khune (Ph.D. (Pursuing), MIT ADT University and Masters in Computer Engineering, RTMNU University). She is working as an Assistant Professor in MIT Art, Design and Technology University, Pune. She has 10 years of teaching experience. Her research areas are embedded system, AI, image processing, and biometrics. She can be contacted at email: priya.khune@mituniversity.edu.in and priyakhune05@gmail.com.

Dr. Nilesh N. Thorat is currently working as a Senior Assistant Professor at MIT Art, Design and Technology University, Pune, Maharashtra, India. His domain of expertise includes AI/ML, computer networking, and image processing. He has having 15 years of teaching experience. His academic interests focus on teaching, research, and practical applications in these areas. He can be contacted at email: nileshthorat4694@gmail.com.

Ashwini G. Shahapurkar (Ph.D. (Pursuing), MIT ADT University and Masters in Computer Engineering, SPPU Pune University) is an Assistant Professor in the Department of Computer Science and Engineering at MIT ADT University, Pune. With over 8 years of teaching experience, she has contributed extensively to research in artificial intelligence, machine learning, and cyber security. She can be contacted at email: ashwini.gs.is003@gmail.com.

Vijaya S. Patil (Ph.D. (Pursuing), MIT ADT University and Masters in Computer Engineering, SPPU Pune University) is an Assistant Professor in the Department of Computer Science and Engineering at MIT ADT University, Pune. With over 19 years of teaching experience, she has contributed extensively to research in artificial intelligence, machine learning, and cyber security. She can be contacted at email: vijaya.patil@mituniversity.edu.in.

Sumit Arun Hirve (Ph.D. in Computer Engineering, VIT AP University) is an Associate Professor in the Department of Computer Science and Engineering at MIT ADT University, Pune. With over 17 years of teaching and industry experience, he has contributed extensively to research in artificial intelligence, machine learning, big data analytics, cyber security, and augmented reality. He can be contacted at email: sumit.hirve@gmail.com.

Aarti P. Pimpalkar awarded M.E. degree from SPPU Pune university in 2013 in Computer Engineering. She is pursuing Ph.D. from MIT Art, Design and Technology University, Loni Kalbhor, Pune, India. She has having 14 years of teaching experience and 6 years of Industry experience. Her research areas include machine learning, deep learning, and image processing. She can be contacted at email: aartipimpalkar@gmail.com.